Structural Characteristics of Aqueous Dispersions of Detonation Nanodiamond and Their Aggregate Fractions as Revealed by SmallAngle Neutron Scattering

ARTICLE *in* THE JOURNAL OF PHYSICAL CHEMISTRY C · JANUARY 2015

Impact Factor: 4.77 · DOI: 10.1021/jp510151b

7 AUTHORS, INCLUDING:

Leonid Bulavin
National Taras Shevchenko University of Kyiv
320 PUBLICATIONS **824** CITATIONS
SEE PROFILE

Andrey V. Rogachev
Joint Institute for Nuclear Research
17 PUBLICATIONS **44** CITATIONS
SEE PROFILE

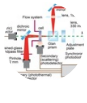

Mikhail Alekseevich Proskurnin
Lomonosov Moscow State University
134 PUBLICATIONS **739** CITATIONS
SEE PROFILE

M. V. Korobov
Lomonosov Moscow State University
77 PUBLICATIONS **952** CITATIONS
SEE PROFILE

THE JOURNAL OF PHYSICAL CHEMISTRY C

Article

pubs.acs.org/JPCC

Structural Characteristics of Aqueous Dispersions of Detonation Nanodiamond and Their Aggregate Fractions as Revealed by Small-Angle Neutron Scattering

Oleksandr V. Tomchuk,[†,‡] Dmitry S. Volkov,[§] Leonid A. Bulavin,[‡] Andrey V. Rogachev,[†] Mikhail A. Proskurnin,[§] Mikhail V. Korobov,[§] and Mikhail V. Avdeev*[,†]

[†]Frank Laboratory of Neutron Physics, Joint Institute for Nuclear Research, Dubna 141980, Russia

[‡]Faculty of Physics, Taras Shevchenko National University of Kyiv, Kyiv 03022, Ukraine

[§]Department of Chemistry, Lomonosov Moscow State University, Moscow 119991, Russia

ABSTRACT: Small-angle neutron scattering was applied for the structure characterization of commercial detonation nanodiamond (DND) suspensions. Two reproducible structural levels corresponding to DND particles (characteristic size ≈ 4 nm) and their developed clusters (characteristic size ≈ 100 nm) showed high size polydispersity. The contrast variation (based on mixtures of light and heavy water) was used to check up the inner structure of DND particles and compare it with the data of the previous analogous experiments. The fractal nature of the observed clusters is discussed in terms of a unique mechanism of the cluster growth in DND suspensions during their synthesis. The structural peculiarities of "light" and "heavy" cluster fractions separated by centrifugation showed the same cluster type at different size scale. The structure−factor effect on the scattering from the concentrated suspensions of "light" and "heavy" clusters is considered to characterize the cluster−cluster interaction in solutions.

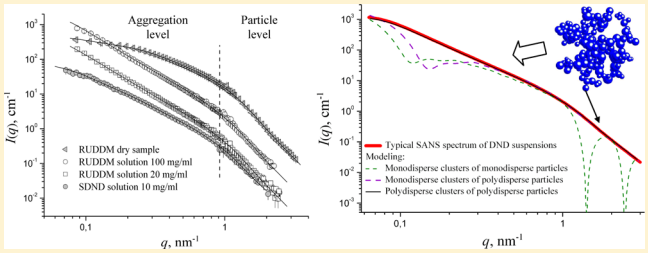

1. INTRODUCTION

Nanodiamonds (diamond crystals with a characteristic size of about 5 nm) are of current interest regarding various industrial[1−3] and biomedical applications.[4−6] Thus, the prospects of nanodiamonds in biomedicine are closely linked with various markers, which use fluorescence or Raman signals for cell imaging, MRI agents, carriers for drug delivery, and other applications.[7,8] The most common way to produce nanodiamonds is based on detonation, when the crystals are formed during the explosion of oxygen-deficit explosives.[9,10] The side effect in the synthesis of detonation nanodiamonds (DND) concerns a significant agglomeration of the primary particles, which occurs mainly through covalent binding between functional groups on the DND surface.[11−13] At present, the decomposition of DND agglomerates is well achieved by different procedures including the stirred-media milling[14,15] or chemical disaggregation.[16] As a result, one obtains a system of primary particles and small aggregates where most of the chemical bonds between the units are broken. Still, the van der Waals and/or electrostatic[10,17] interactions keep DND particles together forming secondary cluster-type structures in dry powders, liquid dispersions, and gels.[18] In DND solutions, there is a tendency toward the formation of developed aggregates, which becomes prominent at high (above 0.1 wt %) concentrations. Correlation was observed between the size distributions of DND species in powders and in water dispersions.[19] Despite the aggregation, the DND suspensions remain stable as a whole, thus showing a weak cluster−cluster interaction. The fractal organization of the aggregates at the length scale up to 100 nm and higher was established by small-angle neutron scattering (SANS).[3] Because of this fact, the clusters can penetrate each other in strongly concentrated solutions and form gel-like nets. Recently, the aggregated DND solutions were fractionated by centrifugation,[7,19,20] which led to the isolation of various fractions with the average size down to 5 nm and less as revealed by the complex analysis including XR diffraction (XRD), high-resolution transmission electron microscopy (HRTEM), and differential scanning calorimetry (DSC). Again, the size characteristics of the fractions were correlated with those of the initial dispersions.[19]

The question that arises in the study of the DND liquid suspensions is how far the aggregate structural characteristics including the size and shape, as well as the character of the cluster−cluster interaction vary in different samples and their fractions, i.e., at different length scales. To clarify this point, in the present work SANS is applied to investigate two commercial DND dispersions and their two (conventionally named "light" and "heavy") fractions isolated with the help of the centrifugation/fractionation procedure. Then the found

Received: October 8, 2014
Revised: December 1, 2014
Published: December 8, 2014

differences are discussed in relation with the previous data of other methods.

2. EXPERIMENTAL SECTION

Two kinds of commercial DND powders, namely, RUDDM (Real-Dzerzhinsk Ltd., Dzerzhinsk, Russia) and SDND (Single-digit nanodiamonds, PlasmaChem GmbH, Berlin, Germany) were used for producing samples for SANS experiments. The two powders have close characteristics quoted by the manufacturers including a crystallite size of ≈ 5 nm (analysis of XRD patterns by the Scherrer equation) and specific surface of ≈ 350 m^2 g^{-1} (BET data); free of additives and milling impurities; negative ζ-potential in suspensions. The aqueous DND suspensions were prepared by dispersing powders in distilled water (deionized water with 18.2 MΩ × cm from Milli-Q Academic system, Millipore, France); then the mixtures were subsequently kept under intensive stirring for 30 min and ultrasound (GRAD 28-35 ultrasound bath, Grad-Technology, Russia) for 1 h. The final concentration was varied within the range of 5−100 mg/mL. The fractionation procedure followed the one described previously.[19] The 100 mg/mL suspensions were placed in 10 mL of polycarbonate Nalgene cells and centrifuged at 25000 rev/min (relative centrifuge force 49000g at r_{max} = 7.01 cm) during 45 or 90 min. In each case, light and heavy fractions of the solutions were formed (Figure 1). These

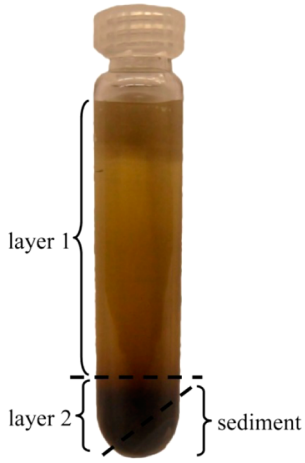

Figure 1. Fractionated sample of RUDDM dispersion after centrifugation.

fractions are denoted as layers 1 and 2, respectively, in Figure 1. Two kinds of fractionated samples were prepared for SANS experiments. First, the two fractions of the solutions were taken by a pipet from the top and bottom layers of the cell. The DND concentration in the fractions was determined by drying small probes of the solutions (at 150 °C) and weighing the precipitates. Second, the fractions were carefully separated and dried at 150 °C. The dry powders obtained from layers 1 and 2 were then used to prepare new aqueous dispersions in the same way as for the initial suspensions.

The SANS experiments were performed on the YuMO time-of-flight small-angle diffractometer at the IBR-2 pulsed reactor of the Frank Laboratory of Neutron Physics, Joint Institute for Nuclear Research, Dubna, Russia.[21,22] The scattered intensity (differential cross section per sample volume) isotropic over the radial angle φ on the large-area detector (size 90 cm) was obtained as a function of the modulus of momentum transfer, q = $(4\pi/\lambda)\sin(\theta/2)$, where θ is the scattering angle and λ is the incident neutron wavelength. The neutron wavelengths within an interval of 0.05−0.5 nm and the sample−detector distances of 4 and 16 m were used to obtain SANS spectra in a q-range of 0.08−2.5 nm^{-1}. The calibration procedure was made using vanadium.[21] The liquid samples as well as dried powder were measured in 1 mm thick flat quartz cuvettes (Hellma).

Both the DND powders and liquid dispersions were studied. The concentration effect on the scattering was followed in the concentration range of 5−100 mg/mL. Several 20 mg/mL dispersions for the contrast variation procedure were prepared by dissolving the initial RUDDM suspension with different mixtures of H_2O/D_2O, so that the relative content of heavy water changed within an interval of 0−80%. As a background, in the case of liquid samples the scattering from the corresponding pure solvents was measured (under the same experimental conditions) and subtracted. In the case of powders the scattering from an empty experimental cell was considered as a background and taken into account in the corrections.

3. RESULTS AND DISCUSSION

3.1. Initial Samples. The principal features of SANS from DND in a dry state and suspensions are illustrated in Figure 2,

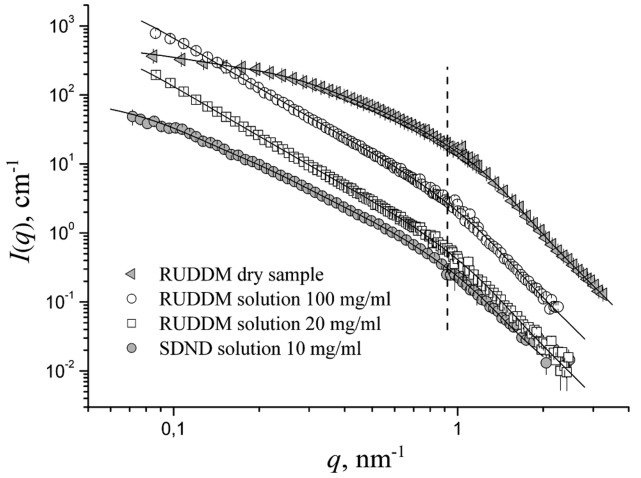

Figure 2. Experimental SANS curves (points) from the RUDDM samples including the initial dry powder and aqueous dispersions with the DND concentration of 100 and 20 mg/mL and the SDND aqueous dispersion with the DND concentration of 10 mg/mL. The solid lines show the fits by the universal exponential/power-law approximations combining two scattering levels (eq 1 or 2). The dashed line conventionally denotes a break between the particle (large q) and the aggregate (low q) scattering levels.

where examples of the experimental scattering curves from the systems under study together with their analysis are given. The behavior of the scattering curves fully repeats the results of the previous SANS experiments for DND powders and suspensions from other producers.[3,23−26] All curves in Figure 2 clearly evidence the two-level organization represented by the particle level (large q-values) and aggregation level (small q-values). In SANS the term "particles" conventionally refers to non-homogeneities or fluctuations of the scattering length density (SLD) distribution over its mean bulk value. In this sense, in powders the scatterers are pores within the packed DND structure,[23] and in liquid suspensions, the scatterers are DND

dx.doi.org/10.1021/jp510151b | J. Phys. Chem. C 2015, 119, 794−802

Table 1. Parameters of the Best Fits of Exponential/Power-Law Approximation (eqs 1 and 2) to the SANS Experimental Curves in Figure 2 and Comparison with the Previous SANS Data[a]

sample	R_g (nm)	R_{gS} (nm)	P	P_S	$\langle R\rangle$ (nm)	σ (nm)
RUDDM powder	14.2(5)	2.13(4)	1.93(9)	4.11(2)		
RUDDM solution 100 mg/mL	>40	2.48(4)	2.40(1)	4.10(2)	1.50(4)	0.56(2)
RUDDM solution 20 mg/mL	>40	2.45(4)	2.39(1)	4.10(2)	1.51(5)	0.57(2)
SDND solution 10 mg/mL	20(1)	2.64(4)	2.31(2)	4.12(6)	1.5(8)	0.6(3)
DND powder (ref 3)	>20	3.2	1.26	4.19		
DND in H_2O (ref 3)	18.3(1)	2.9	2.34	4.13	1.48(6)	0.62(3)
DND in H_2O (ref 26)	17.9(2)	3.30(8)	2.45	4.12(4)	1.3(1)	0.58(6)

[a]Parameters of the log-normal size distribution, $\langle R\rangle$ and σ, for DND particles are calculated based on the parameters of the exponential/power-law approximation following refs 26 and 27. The powder samples are skipped in these calculations since the procedure is incorrect for the pores.

particles themselves.[3] In both cases, the scatterers can be considered as basic structural units, which form the next structural level (aggregates) reflected in SANS curves as an additional scattering level corresponding to larger sizes as compared to the DND particles. The important (from the scattering viewpoint) peculiarity of all the experimental curves in Figure 2 is their smoothness over the q-interval corresponding to the particle level, i.e., the absence of fringes in the scattering patterns characteristic for monodisperse particles. This is a strong evidence of high polydispersity at this level. The specific features that can be distinguished in the curves are the power-law type scattering at both levels (they are illustrated by solid lines, which have linear behavior in the double logarithmic scale) and a crossover between the two scattering regimes at $q \approx 0.9$ nm^{-1} corresponding to the size of the basic units. Using the condition $q \approx 2\pi/L$ connecting the real and reciprocal spaces, where L is the characteristic size, one obtains $L \approx 7$ nm, which is consistent with the smaller crystallite size of DND found by X-ray diffraction because of the presence of some graphite-like shell in the DND structure (see, e.g., ref 27). The scattering curves in Figure 2 are analyzed in the frame of the universal exponential/power-law approximation,[28] which was shown[3,23] to be very efficient in the structural analysis of the systems similar to those studied here. The scattered intensity, $I(q)$, is modeled as

$$I(q) = G\exp(-q^2R_g^2/3) + B\exp(-q^2R_{gS}^2/3)(\mathrm{erf}(1.1qR_g/6^{1/2})/q)^P + G_S\exp(-q^2R_{gS}^2/3) + B_S(\mathrm{erf}(qR_{gS}/6^{1/2})/q)^{P_S} \quad (1)$$

Here, like in the previous works[3,23] employing this expression, the parameters with the "S" index correspond to the particle level and the parameters without any indexes describe the structural level of the aggregates. Each level is represented by two terms in eq 1, which are described by the Guinier law (scattering from the shape of the object) and the power law (scattering from the spatial correlations within the object). Thus, R_{gS} and R_g are the radii of gyration corresponding to the particle and aggregation levels, respectively; G_S and G are the corresponding forward scattered intensities; the P_S exponent is related to the surface structure of the particles, while P is equal to the mass fractal dimension of the aggregates. The scattering from the RUDDM powder sample and the SDND liquid suspension in Figure 2 fits well into eq 1. In the case of the RUDDM liquid suspensions the aggregate size is out of the used instrumentation limit with respect to the minimum q-value, q_{min}, covered in the experiment. Again, using the relation between the real and reciprocal spaces one can estimate the characteristic cluster size as $L > 2\pi/q_{min} \approx 75$ nm. So, since the Guinier regime is not observed at the aggregation level, eq 1 can be modified in the following way:[3,23]

$$I(q) = B\exp(-q^2R_{gS}^2/3)(1/q)^P + G_S\exp(-q^2R_{gS}^2/3) + B_S(\mathrm{erf}(qR_{gS}/6^{1/2})/q)^{P_S} \quad (2)$$

The resulting fits of eqs 1 and 2 are shown in Figure 2; the most informative parameters of the fits are collected in Table 1. As it was mentioned above, the P-values for all samples correspond to the mass fractal regime ($P < 3$), which differs significantly from that observed in dry DND powders. This difference was explained previously[3] by different packing densities of pores in powders and nanocrystallites in suspensions.

Both the DND particles and pores have the same interface, which is well reflected at the particle level for all the samples in Figure 2 revealing close exponents, $P_S \approx 4.1$, slightly larger than the Porod exponent $P_S = 4$ corresponding to a smooth boundary. In the theory of small-angle scattering the case $P_S > 4$ is interpreted in terms of a specific modulation of the scattering length density on the particle surface known as the diffusive interface.[25,26] It is characterized by the β-exponent ($P_S = 4 + 2\beta$, $0 < \beta < 1$). From the experimentally obtained P_S-values we find $\beta = 0.05(1)$ (RUDDM) and $\beta = 0.06(3)$ (SDND). According to the experimental errors, the excess of the P_S-exponent over 4 is essential, which is fully consistent with the previous SANS data from other DND dispersions.[3,23,25,26] Recently, such kind of interface was associated with a comparatively wide spatial transition of carbon from diamond in the DND particle center to graphite-like states at the surface.[26,27] Using the continuous approximation to the radially averaged SLD profile, $\rho(r)$, within DND particles and assuming the particle size distribution function to be of the log-normal type,[26,27] one can directly obtain the characteristics of the particle size distribution (mean radius and the mean square deviation) from the experimental curves. The found parameters are collected in Table 1.

It should be noted that from the scattering viewpoint the aggregation level of all liquid DND dispersions studied by SANS in the previous and current works is characterized by a close fractal organization independent of the dispersion origin (see Table 1). This is indicative of a specific mechanism of the aggregate growth in this kind of systems; presumably, in accordance with the observed mass fractal dimension of the clusters, $P \approx 2.4$, the diffusion-limited aggregation (DLA)[29] takes place. In this case, the smoothed cluster scattering level satisfying the power-law regime suggests a wide cluster size distribution. Otherwise, for monodisperse fractal clusters

dx.doi.org/10.1021/jp510151b | J. Phys. Chem. C 2015, 119, 794−802

formed in the DLA process one can expect a specific "valley" in the scattering curve with a lower than the power-law dependence intensity.[30,31] The point is illustrated in Figure 3.

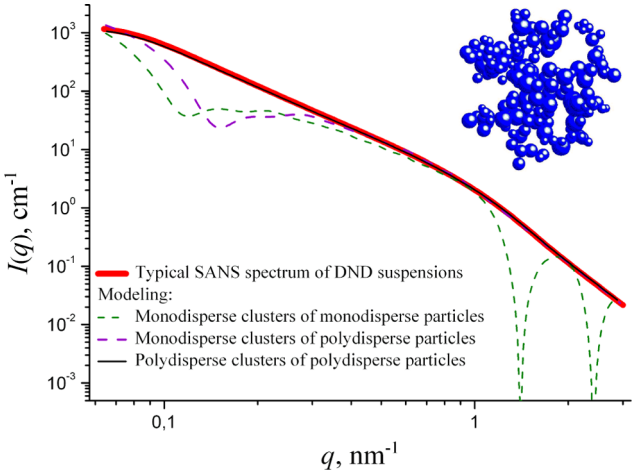

Figure 3. Calculated scattering curves from the model DLA clusters of homogeneous spherical units generated by the algorithm from ref 32 in various regimes with respect to the monodispersity/polydispersity of structural units and the clusters themselves. The inset shows the example of a cluster with polydisperse structural units. The curves are compared with the model two-level scattering curve from a DND suspension calculated according to eq 1. The parameters used in the cluster generation: for monodisperse units, R = 3.2 nm; for monodisperse clusters, R_{cl} = 45 nm, k = 1.1; for polydisperse units with log-normal size distribution, $\langle R\rangle$ = 1.5 nm, σ = 0.5 nm; for polydisperse clusters with log-normal size distribution, $\langle R_{cl}\rangle$ = 100 nm, σ_{cl} = 25 nm, k = 1.

The same figure additionally shows the polydispersity effect of the DND particles on the scattering. The model three-dimensional DLA clusters of spherical homogeneous particles were generated according to the sequential algorithm by Filippov et al.[32] The stepwise generation in this case is based on the attachment of the Nth particle to a cluster already consisting of $N-1$ particles in such a way as to make the formed cluster satisfy the general scaling equation for fractals:

$$N = k(R_{cl}/R)^D \tag{3}$$

where D is the cluster fractal dimension; R is the particle radius; R_{cl} is the cluster radius measured from the center of mass of the cluster; and k is the fractal prefactor (lacunarity). In practice, eq 3 is transformed[32] into the condition restricting the position, $\vec{r}_N$, of the Nth particle when attaching the cluster of $N-1$ particles with respect to the cluster center of mass, $\vec{r}^{\,0}_{N-1}$:

$$(\vec{r}_N - \vec{r}^{\,0}_{N-1})^2 = \frac{N^2R^2}{N-1}\left(\frac{N}{k}\right)^{2/D} - \frac{NR^2}{N-1} - NR^2\left(\frac{N-1}{k}\right)^{2/D} \tag{4}$$

In the present work, the algorithm was extended to polydisperse structural units composing clusters, so eq 4 was modified to take the form

$$(\vec{r}_N - \vec{r}^{\,0}_{N-1})^2 = \frac{M_N{}^2}{m_N M_{N-1}} a_N{}^2\left(\frac{N}{k}\right)^{2/D} - \frac{M_N}{M_{N-1}}\left(\frac{3}{5}\right)R_N{}^2 - \frac{M_N}{m_N}a_{N-1}{}^2\left(\frac{N-1}{k}\right)^{2/D} \tag{5}$$

Here, together with the radius of the Nth particle, R_N, its mass, m_N, is introduced, which is for homogeneous particles proportional to the particle volume; then, the total masses of the cluster, M_N and M_{N-1}, at the steps N and $N-1$, respectively, are related as $M_N = M_{N-1} + m_N$; the coefficients a_N and a_{N-1} are the mean particle radii, i.e., the results of averaging over the particles included in the cluster after steps N and $N-1$, respectively. An example of the model cluster made of polydisperse units is given in the inset to Figure 3. The size of the model clusters was arbitrary chosen in the range of around 100 nm (the aggregation number of about 180 for the mean particle size of 3 nm) to repeat the situation with the concentrated RUDDM suspensions showing the most pronounced power-law behavior at the cluster scattering level over a wide q-interval. The scattering curves from the model clusters were calculated by using the Debye formula (see, e.g., ref 33):

$$I(q) \approx \sum_{j=1}^{N}\sum_{k=1}^{N} F(q, R_j)F(q, R_k)\,\sin(q|\vec{r}_j - \vec{r}_k|)/(q|\vec{r}_j - \vec{r}_k|) \tag{6}$$

where $\vec{r}_i$ and $\vec{r}_j$ are the radii-vectors of the ith and jth spherical units in the cluster and $F(q,R_i) = 3(\sin(qR_i) - qR_i\cos(qR_i))/(qR_i)^3$ is the scattering form-factor of the ith unit with the radius R_i. The obtained curves are shown in Figure 3. The corresponding input parameters of the algorithm are indicated in the caption to Figure 3. When comparing the model curves with a typical scattering curve from liquid DND dispersions calculated according to eq 1 using the same cluster size, one can clearly see that the monodisperse cases are characterized by significant deviations from the power-law type scattering at both the particle and cluster levels. The polydispersity for the DND particles was modeled in Figure 3 using the parameters of the particle size distribution function known from the analysis done above. The modeling of the cluster size distribution is mainly of illustrative character here being based on some arbitrarily chosen mean cluster size. It does not claim to be a unique function satisfying the scattering at the cluster level and just shows a principal possibility to obtain a smoothed scattering curve in the discussed q-interval in contrast to the monodisperse case.

To some extent the indications of a unique mechanism of the aggregate growth in DND suspensions provide support for a recently proposed[17] scheme of DND interaction in solutions as a result of surface modulations in the electrostatic potential. The modeling shows that the charged facets of regularly shaped (truncated octahedral or cuboctahedral) diamond nanocrystallites have alternating signs, which leads to a strong facet−facet attraction and thus reproducible clusters from the viewpoint of the scaling symmetry. The lower value of the P exponent for the SDND suspension as compared to that for the RUDDM sample is explained by the cluster size effect in the first case, which is reflected in the scattering curve as a strong deviation from the power-law type dependence at small q-values (see Figure 2) corresponding to a transition to the Guinier scattering regime. For the polydisperse clusters in the

dx.doi.org/10.1021/jp510151b | J. Phys. Chem. C 2015, 119, 794−802

solution this transition is rather wide with respect to the q-range, so the q-interval, where the pure power-law dependence takes place, is significantly narrower for the SDND suspension and affected by the transition to the Guinier scattering regime. This causes systematic deviations in the P-parameter toward lower values.

The interaction between the aggregates can result in specific correlations at the scale of about 100 nm and higher in sufficiently concentrated solutions. In Figure 2 the corresponding structure-factor effect is slightly visible for the 100 mg/mL RUDDM sample as a deviation from the power-law type scattering toward lower intensity at the smallest q-values. The fact that it is not a consequence of the finite aggregate size is proved by diluting the system down to 20 mg/mL, where this effect disappears. At the same time, the discussed type of deviations retains for diluted SDND suspensions (example is given in Figure 2), which means that in this case they refer to the real aggregate size (given in Table 1). The obtained results on the aggregate characteristic sizes are in qualitative consistency with the reported[19] data of DLS and DSC on the same types of DND suspensions, which also proved better dispergating properties of SDND with respect to the cluster formation. The full comparison that would include the quantitative analysis is hardly possible since the aggregate formation is rather sensitive to the conditions in the preparation procedure.[19] There are several additional factors, which complicate the comparison between DLS and SANS. DLS measurements are made with sufficiently diluted systems that are naturally characterized by smaller aggregation. Then, the calculation of the hydrodynamic size from the diffusion coefficient provided by DLS assumes a compact shape of the studied object, which is not true for the developed fractal clusters in DND solutions. Until now, in the case of fractal clusters there is no clear way how to relate the observed diffusion coefficient and the cluster size. The situation is more complicated if one takes the polydispersity of basic structural units composing clusters into account.

To prove completely the similarity of DND particles in different suspensions, we repeat here the SANS contrast variation on the RUDDM dispersion as in refs 3, 25, and 26 The change in the scattering with a different content of D_2O in the solvent for the 20 mg/mL suspensions is followed in Figure 4. The character of this change (monotonous decrease in the total scattered intensity at the aggregation level with the P parameter remaining constant and a slight increase in the P_S-exponent at the particle level) fully reproduces the behavior observed previously. Again, to avoid the effect of residual solvent scattering, we use here the dependence of the intensity at the minimum q-value covered, I_0, on the D_2O content in the solvent to find out the match point of the aggregates and, consequently, the particles composing them. The corresponding plot of the square root of I_0 against the calculated solvent SLD is given in the inset to Figure 4. The graph fits well a linear dependence whose interception with the abscissa (match point) gives the mean scattering length density of DND particles $\overline{\rho}$ = 11.0(4) × 10^{10} cm^{-2}. As compared to the previous results,[3] it is closer to SLD of diamond, ρ_0 = 11.8(3) × 10^{10} cm^{-2}, known from its crystalline structure, but still the difference is significant. The obtained value agrees well with the value of $\overline{\rho}$ = 10.8(4) × 10^{10} cm^{-2} followed from the continuous approximation to the SLD profile[27] using SLD of diamond and experimentally found β.

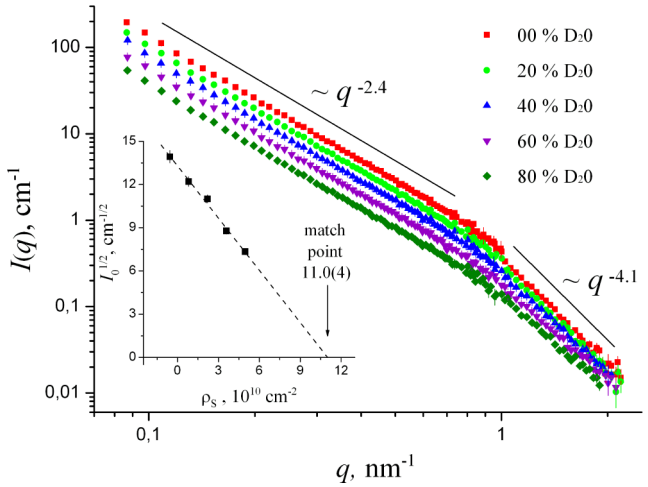

Figure 4. SANS contrast variation for the 20 mg/mL RUDDM dispersions prepared from the initial 100 mg/mL dispersion diluted five times with different D_2O/H_2O mixtures. The volume fractions of D_2O in the final solutions are given in the legends to the experimental scattering curves. The specific power-law type scattering regimes are shown by solid lines. The inset shows the experimentally found values of $I_0^{1/2}$ against the calculated solvent SLD with the linear extrapolation to the match point.

3.2. Fractionated Samples. The phase separation under centrifugation is followed in Figure 5a, where the SANS curves from the light and heavy fractions of the 100 mg/mL RUDDM suspension after two different times of centrifugation are given. The two fractions show a difference regarding the scattering at the aggregation level. The light fraction is characterized by significantly smaller aggregates; the corresponding scattering can be well described by the Guinier approximation in the region of small q-values, which makes it possible to apply the indirect Fourier transform[34,35] and represent the correlations in the systems in terms of the pair distance distribution (PDD) functions, $p(r)$, comprising the size characteristics such as Z-average of the radius of gyration and maximum size. It can be clearly seen in Figure 6 where the PDD functions (which combine information about the particle and cluster size distributions) of the corresponding curves are compared with that for the SDND suspension. Because of a significantly smaller volume in comparison with the clusters observed in the initial suspensions, the discussed associates of the light fractions have a negligible effect on the total scattering (which is proportional to the squared volume of the scatterers) in the experiments with the initial suspensions (Figure 2). As it follows from Figure 5a, the longer centrifugation results in an effectively smaller size of the aggregates in the light fraction, which is naturally consistent with a stronger separation of the clusters over their size. Despite the difference in the aggregate state in the initial RUDDM and SDND suspensions, the size characteristics of the light fractions after 90 min centrifugation are close for both types of dispersions. The comparison of the corresponding scattering curves referred to one concentration is given in Figure 5b. The mean aggregation number of the clusters in these fractions is about 10 as estimated from the ratio between the forward scattered intensities measured in the experiment and calculated under assumption that all DND particles are separated in the solution. It is clear that the fractal properties are not so distinguishable at such small aggregation numbers, so there are strong deviations from the power-law

dx.doi.org/10.1021/jp510151b | J. Phys. Chem. C 2015, 119, 794−802

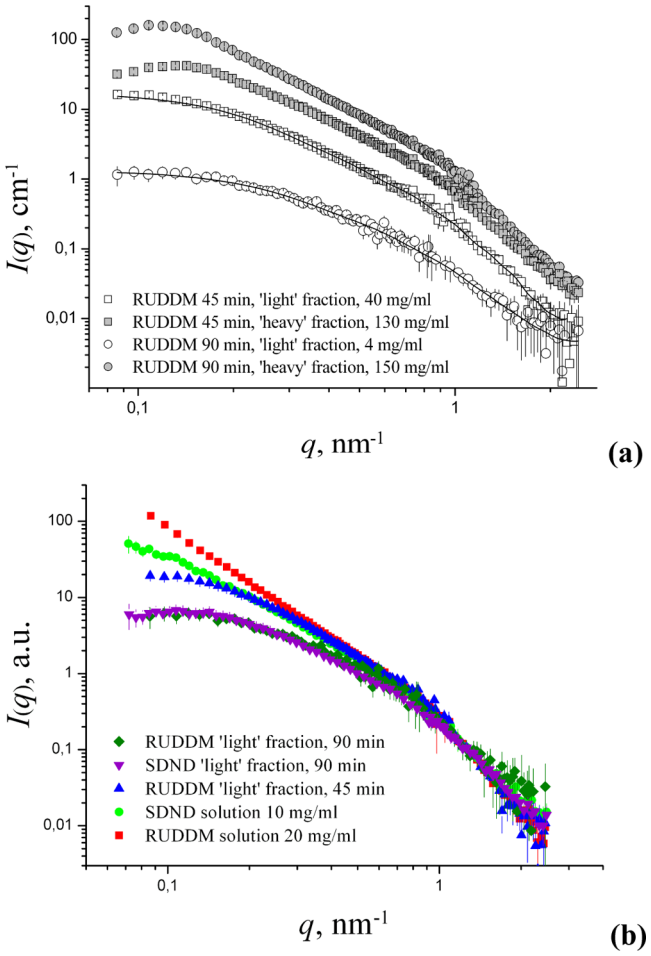

Figure 5. (a) Experimental SANS curves from the heavy and light fractions of 100 mg/mL RUDDM suspension under centrifugation. The centrifugation time is indicated in the sample legend. The solid lines are the model curves obtained by the indirect Fourier transform for light fractions. (b) Comparison of the experimental SANS curves from different samples referred to one DND concentration.

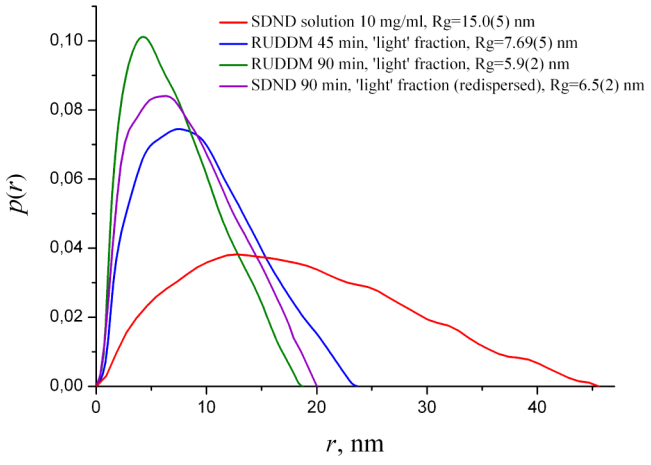

Figure 6. Pair distance distribution functions (calibrated to unit) as a result of the treatment of the SANS curves from the light fractions by the indirect Fourier transform. The obtained values of radii of gyration are indicated.

type scattering because of the cluster size effect. In addition, because of a decrease in the mean volume (as compared to the heavy fractions), the scattered intensity drops and the incoherent background from the solvent markedly affects the precision of the parameters in the exponential/power-law approximation (eqs 1 and 2). At the same time a very similar behavior of the scattered intensity at the particle level is observed for all dispersions and fractions under study. In Figure 5b it is illustrated by comparing the scattering curves from some light fractions and the initial DND suspensions. The given comparison shows that at the aggregation level the only difference between the scattering from all the samples studied concerns the cluster size effect. In this connection, one can state that the mechanism of the cluster growth is the same for small and large clusters in different dispersions. This also proves that the aggregates are stable regarding the redispersion procedure and centrifugation and thus are formed in the course of the synthesis of liquid suspensions from DND powders. The synthesis process includes the oxidation of the DND particles in liquid media, which results in electrostatic stabilization of suspensions. It competes with the aggregation; as a result, some cluster distribution over a wide range of sizes is stabilized. Our study strongly confirms the hypothesis about a unique mechanism of the aggregate formation during the synthesis and, consequently, the same aggregate structure in DND liquid dispersions as a class of colloidal systems. The synthesis procedures followed by different producers are characterized by different stabilization rates, which results in different cluster size distributions in liquid dispersions of DND. In this sense the studied here SDND aqueous dispersions show better stabilization as compared to RUDDM dispersions with respect to the width of the cluster size distribution. On the basis of DLS and DSC analysis,[19] it was shown that in SDND a fraction of nonaggregated DND particles is present, which can be separated after 360 min centrifugation. However, the concentration of such particles is too low to be detected by SANS against the comparatively high incoherent scattering from hydrogen in the aqueous carrier. In fact, the signal/background ratio in SANS restricts the centrifugation time to separate the light fraction from the viewpoint of size and concentration of clusters remaining in the fraction. The chosen here maximum centrifugation time is a limit when the particle level in the SANS curves (large q-values) can be detected and treated with sufficient statistics.

As to the heavy fractions, the corresponding curves in Figure 5a repeat those from the initial suspensions over most of the q-interval covered, which means that these fractions consist mainly of the large developed clusters observed in the initial solutions (Figure 2). A significant difference is observed only in the initial parts of the curves. One can see that the structure–factor effect, i.e., the deviation from the power-law type scattering at the smallest q-values, in the heavy fractions is more pronounced as compared to the initial suspensions (Figure 2). It is characterized by the appearance of peaks at $q < 0.2$ nm^{-1} corresponding to the correlation length of about $2\pi/q_{peak} = 45$ nm. This is a consequence of the higher particle concentration upon centrifugation and can be interpreted as a result of the interpenetration of the developed aggregates in full agreement with the previous conclusions on the concentrated solutions with developed DND clusters.[3]

The better dispergating properties of SDND were used to study the interaction character of the small aggregates in the light fraction. For this purpose, the dried powder from this fraction after 90 min centrifugation was redispersed into water in a wide concentration range of 5–100 mg/mL. The scattered

dx.doi.org/10.1021/jp510151b | J. Phys. Chem. C 2015, 119, 794–802

intensity from the corresponding solutions is followed in Figure 7. It is important that besides the initial parts the character of

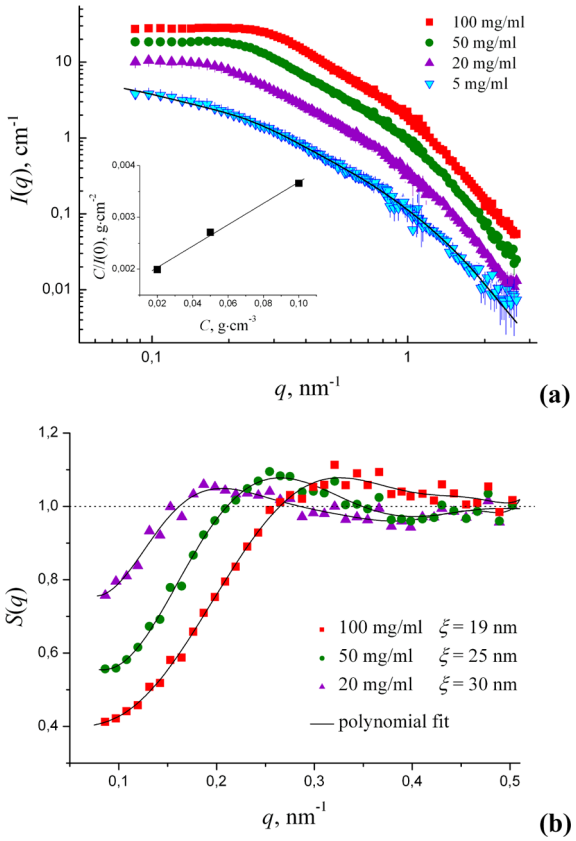

Figure 7. (a) SANS curves from the redispersions of the light fraction from the SDND suspension in water at different concentrations (indicated in the legends). The solid line shows the IFT fit (the corresponding PDD function is given in Figure 5. The inset shows the Zimm plot with the corresponding linear fit according to eq 7. (b) Effective structure factors according to eq 8. For a convenient view of the first structural peak, the $S(q)$ plots are approximated by polynomial curves; the correlation length, ξ, corresponding to the interaction peak in $S(q)$ is given in the legend.

the curves does not change with the concentration. This strongly proves that the clusters precipitated in the light fraction under drying retain their structure after redispergation into the liquid carrier, thus showing tight contacts of DND particles within the aggregates. The region of small q-values in the scattering curves is influenced by the structure−factor effect, which leads to significant deviations from the Guinier-type scattering because of the interaction between the aggregates themselves (Figure 7a). The type of the interaction was concluded from the concentration dependence of the ratio C/I_0 (see the inset in Figure 7a), where C is the mass fraction of the dissolved DND, and the forward scattered intensity, I_0, was estimated by using the far left points of the scattering curves. This dependence is described by the Zimm equation[36] as

$$C/I_0 = K + A_2LC \quad (7)$$

where K and L are some positive constants, and A_2 is the second virial coefficient, whose sign determines the interaction type. Here, the Zimm plot shows a positive slope corresponding to $A_2 > 0$, which means the repulsive type of interaction. The structure-factor is estimated as

$$S(q) = (I(q, C)/C)/(I(q, C_1 \to 0)/C_1) \quad (8)$$

where C_1 is the minimum concentration covered in the experiment. The found $S(q)$ function (Figure 7b) is characterized by a clearly visible peak whose position, q_{peak}, shifts toward higher q-values with increasing DND concentration, thus showing a decrease in the correlation length, $\xi \approx 2\pi/q_{peak}$, corresponding to the cluster−cluster short-range interaction. The modeling of the structure factor faces difficulties caused by high polydispersity of the aggregates as concluded above. The attempt to approximate $S(q)$ by the hard sphere models for polydisperse systems[37] failed. This can be explained by the fact that the developed aggregates in the suspensions are far from the compact spherical-like objects (e.g., see asymmetry in the PDD functions in Figure 6), and there is an additional contribution into the interaction potential from the charge repulsion partially screened by the polar solvent. At the highest concentration covered, the correlation length (about 20 nm as it follows from Figure 7b) approaches the characteristic aggregate size (which is, because of the fractal structure, exceeding 17 nm, the size of the equivalent packed spherical aggregate with the R_g-value for the SDND light fraction indicated in Figure 6), that is the aggregates can come comparatively close to each other. Still, the charge on the DND surface prevents the aggregates from agglomerating. The considered structure−factor effect is similar to that previously observed[3] for nonfractionated DND suspensions (aggregate size above 40 nm), which pointed to an even closer approach and possible interpenetration of the branched aggregates at the concentrations around 100 mg/mL. One can see a trace of this effect for the 100 mg/mL RUDDM solution in Figure 2 at small q-values and its stronger manifestation for the heavy fractions of the RUDDM solution with the characteristic cluster size of about 100 nm and concentrations above 100 mg/mL in Figure 5a discussed above.

4. CONCLUSIONS

To summarize, the SANS data prove the presence of the developed clusters of DND particles in the corresponding aqueous dispersions irrespective of the producer. With the wide size distribution for the DND particle (mean size 3 nm, polydispersity index ≈ 40%), high polydispersity (size range from below 10 nm to above 100 nm) has been revealed for the DND clusters as well. The clusters are stable in time and retain their structure after the suspensions are dried and the sediments are redispersed into water. All these are indicative of the fact that the clusters are formed during the synthesis of the initial DND suspensions, which includes disaggregation, purification, and oxidation of the DND powders. For the investigated here commercial RUDDM and SDND dispersions, the only principal structural difference observed concerns the final cluster size distribution, which corresponds to significantly smaller sizes (radius of gyration, 20 nm against >40 nm) in the second case. If one takes into account the fractal dimension of the observed clusters ($D \approx 2.4$), the corresponding mechanism of the cluster growth can be associated with the diffusion-limited aggregation. This mechanism seems to be unique for liquid DND dispersions as a class of colloidal systems. The type of the cluster structure retains at different size scales. The various cluster fractions can be separated by centrifugation without any significant effect on the cluster structure. The

dx.doi.org/10.1021/jp510151b | J. Phys. Chem. C 2015, 119, 794−802

effective interaction radius of the stable branched and charged clusters strongly depends on the concentration and cluster size. In heavy fractions containing clusters with the characteristic size of about 100 nm the correlation length is comparable with the cluster size at the DND concentrations above 100 mg/mL, i.e., the interpenetration of the clusters takes place.

AUTHOR INFORMATION

Corresponding Author

*Phone: +7 496 21 62 674. Fax: +7 496 21 65 484. E-mail: avd@nf.jinr.ru.

Author Contributions

The manuscript was written through the contributions of all authors.

Notes

The authors declare no competing financial interest.

ACKNOWLEDGMENTS

The financial support of RFBR is acknowledged (grant 12-02-00649).

REFERENCES

(1) Hanada, K.; Matsuzaki, K.; Sano, T. Nanocrystalline Diamond Films Fabricated by Sol-Gel Technique. *Surf. Sci.* **2007**, *601*, 4502−4505.

(2) Baidakova, M.; Vul', A. New Prospects and Frontiers of Nanodiamond Clusters. *J. Phys. D* **2007**, *40*, 6300−6311.

(3) Avdeev, M. V.; Rozhkova, N. N.; Aksenov, V. L.; Garamus, V. M.; Willumeit, R.; Ōsawa, E. Aggregate Structure in Concentrated Liquid Dispersions of Ultrananocrystalline Diamond by Small-Angle Neutron Scattering. *J. Phys. Chem. C* **2009**, *113*, 9473−9479.

(4) Holt, K. B. Diamond at the Nanoscale: Applications of Diamond Nanoparticles from Cellular Biomarkers to Quantum Computing. *Philos. Trans. R. Soc. London, Ser. A* **2007**, *365*, 2845−2861.

(5) Chao, J. I.; Perevedentseva, E.; Chung, P. H.; Liu, K. K.; Cheng, C. Y.; Chang, C. C.; Cheng, C. L. Nanometer-Sized Diamond Particle as a Probe for Biolabeling. *Biophys. J.* **2007**, *93*, 2199−2208.

(6) Liu, K. K.; Cheng, C. L.; Chang, C. C.; Chao, J. I. Biocompatible and Detectable Carboxylated Nanodiamond on Human Cell. *Nanotechnology* **2007**, *18*, 325102(10pp).

(7) Williams, O. A.; Hees, J.; Dieker, C.; Jager, W.; Kirste, L.; Nebel, C. E. Size Dependent Reactivity of Diamond Nanoparticles. *ACS Nano* **2010**, *4*, 4824−4829.

(8) Chen, M.; Zhang, X.-Q.; Man, H. B.; Lam, R.; Edward, K.; Chow, E. K.; Ho, D. Nanodiamond Vectors Functionalized with Polyethylenimine for siRNA Delivery. *J. Phys. Chem. Lett.* **2010**, *1*, 3167−3171.

(9) Shenderova, O. A.; Zhirnov, V. V.; Brenner, D. W. Carbon Nanostructures. *Crit. Rev. Solid State Mater. Sci.* **2002**, *27*, 227−356.

(10) Ōsawa, E. Monodisperse Single Nanodiamond Particulates. *Pure Appl. Chem.* **2008**, *80*, 1365−1379.

(11) Chiganova, G. A. Aggregation of Particles in Ultradispersed Diamond Hydrosols. *Colloid J. Russ. Acad. Sci.* **2000**, *62*, 238−243.

(12) Lin, E. E. Aggregation of Crystalline Clusters in the Shock Wave Front Propagating through Condensed Species. *Sov. J. Chem. Phys.* **1994**, *12*, 404−409.

(13) Aleksenskii, A. E.; Osipov, V. Y.; Dideykin, A. T.; Vul', A. Y.; Adreaenssens, G. J.; Afanasev, V. V. Ultradisperse Diamond Cluster Aggregation Studied by Atomic Force Microscopy. *Technol. Phys. Lett.* **2000**, *26*, 819−821.

(14) Krüger, A.; Kataoka, F.; Ozawa, M.; Fujino, T.; Suzuki, Y.; Aleksenskii, A. E.; Vul', A. Y.; Ōsawa, E. Unusually Tight Aggregation in Detonation Nanodiamond: Identification and Disintegration. *Carbon* **2005**, *43*, 1722−1730.

(15) Eidelman, E. D.; Siklitsky, V. I.; Sharonova, L. V.; Yagovkina, M. A.; Vul', A. Y.; Takahashi, M.; Inakuma, M.; Ozawa, M.; Ōsawa, E. A Stable Suspension of Single Ultrananocrystalline Diamond Particles. *Diamond Relat. Mater.* **2005**, *14*, 1765−1769.

(16) Fedutik, Y.; Antipovn, A.; Maltseva, E.; Kalachev, A.; Gubarevich, T. Non-Aggregated Detonation Nanodiamonds. Proceedings of 3rd International Symposium of Detonation Nanodiamonds: Technology, Properties and Applications, St. Petersburg, Russia, July 01−04, 2008; pp 65−72.

(17) Barnard, A. S. Self-Assembly in Nanodiamond Agglutinates. *J. Mater. Chem.* **2008**, *18*, 4038−4041.

(18) Korobov, M. V.; Batuk, M. M.; Avramenko, N. V.; Ivanova, N. I.; Rozhkova, N. N.; Ōsawa, E. Aggregate Structure of "Single-Nano Buckydiamond" in Gel and Dried Powder by Differential Scanning Calorimetry and Nitrogen Adsorption. *Diamond Relat. Mater.* **2010**, *19*, 665−671.

(19) Korobov, M. V.; Volkov, D. S.; Avramenko, N. V.; Belyaeva, L. A.; Proskurnin, M. A. Improving the Dispersity of Detonation Nanodiamond: Differential Scanning Calorimetry as a New Method of Controlling the Aggregation State of Nanodiamond Powders. *Nanoscale* **2013**, *5*, 1529−1536.

(20) Peng, W.; Mahfouz, R.; Pan, J.; Hou, Y.; Beaujuge, P.; Bakr, O. Gram-Scale Fractionation of Nanodiamonds by Density Gradient Ultracentrifugation. *Nanoscale* **2013**, *5*, 5017−5026.

(21) Ostanevich, Y. M. Time-of-Flight Small-Angle Scattering Spectrometers on Pulsed Neutron Sources. *Macromol. Chem. Macromol. Symp.* **1988**, *15*, 91−103.

(22) Serdyuk, I. N. Neutron-Scattering in the Ribosome Structure. *Phys. B* **1997**, *234*, 188−192.

(23) Avdeev, M. V.; Aksenov, V. L.; Rosta, L. Pressure Induced Changes in Fractal Structure of Detonation Nanodiamond Powder by Small-Angle Neutron Scattering. *Diamond Relat. Mater.* **2007**, *16*, 2050−2053.

(24) Tomchuk, O. V.; Avdeev, M. V.; Bulavin, L. A.; Aksenov, V. L.; Garamus, V. M. Small-Angle Neutron Scattering by Fractal Clusters in Aqueous Dispersions of Nanodiamonds. *Phys. Particle Nucl. Lett.* **2011**, *8*, 1046−1048.

(25) Tomchuk, O. V.; Avdeev, M. V.; Aksenov, V. L.; Garamus, V. M.; Bulavin, L. A.; Ivashevskaya, S. N.; Rozhkova, N. N.; Schreiber, N.; Schreiber, J. Comparative Structural Characterization of the Water Dispersions of Detonation Nanodiamonds by Small-Angle Neutron Scattering. *J. Surf. Invest.* **2012**, *6*, 821−824.

(26) Tomchuk, O. V.; Bulavin, L. A.; Aksenov, V. L.; Garamus, V. M.; Ivankov, O. I.; Vul', A. Y.; Dideikin, A. T.; Avdeev, M. V. Small-Angle Scattering from Polydisperse Particles with a Diffusive Surface. *J. Appl. Crystallogr.* **2014**, *47*, 642−653.

(27) Avdeev, M. V.; Aksenov, V. L.; Tomchuk, O. V.; Bulavin, L. A.; Garamus, V. M.; Ōsawa, E. The Spatial Diamond-Graphite Transition in Detonation Nanodiamond as Revealed by Small-Angle Neutron Scattering. *J.Phys.: Condens. Matter* **2013**, *25*, 445001(7pp).

(28) Beaucage, G. Small-Angle Scattering from Polymeric Mass Fractals of Arbitrary Mass-Fractal Dimension. *J. Appl. Crystallogr.* **1996**, *29*, 134−149.

(29) Witten, T. A.; Sander, L. M. Diffusion-Limited Aggregation. *Phys. Rev. B* **1983**, *27*, 5686−5697.

(30) Oh, C.; Sorensen, C. M. Structure Factor of Diffusion-Limited Aggregation Clusters: Local Structure and Non-Self-Similarity. *Phys. Rev. E* **1998**, *57*, 784−790.

(31) Mandelbrot, B. B. Plane DLA Is Not Self-Similar; It Is a Fractal that Becomes Increasingly Compact as it Grows? *Phys. A* **1992**, *191*, 95−107.

(32) Filippov, A. V.; Zurita, M.; Rosner, D. E. Fractal-Like Aggregates: Relation between Morphology and Physical Properties. *J. Colloid Interface Sci.* **2000**, *229*, 261−273.

(33) Pedersen, J. S. Analysis of Small-Angle Scattering Data from Polymeric and Colloidal Systems: Modelling and Least-Squares Fitting. *Adv. Colloid Interface Sci.* **1997**, *70*, 171−210.

(34) Pedersen, J. S.; Hansen, S.; Bauer, R. The Aggregation Behavior of Zinc-Free Insulin Studied by Small-Angle Neutron Scattering. *Eur. Biophys. J.* **1994**, *22*, 379−389.

(35) Oliveira, C. L. P.; Behrens, M. A.; Pedersen, J. S.; Erlacher, K.; Otzen, D. E.; Pedersen, J. S. A SAXS Study of Glucagon Fibrillation. *J. Mol. Biol.* **2009**, *387*, 147−161.
(36) Zimm, B. H. The Scattering of Light and the Radial Distribution Function of High Polymer Solutions. *J. Chem. Phys.* **1948**, *16*, 1093−1099.
(37) Frenkel, D.; Vos, R. J.; de Kruif, C. G.; Vrij, A. Structure Factors of Polydisperse Systems of Hard Spheres: a Comparison of Monte Carlo Simulations and Percus-Yevick Theory. *J. Chem. Phys.* **1986**, *84*, 4625−4630.